4-8-2013

The Cluster and Field Galaxy Active Galactic Nucleus Fraction at Z = 1-1.5: Evidence for a Reversal of the Local Anticorrelation between Environment and AGN Fraction

Paul Martini
The Ohio State University

E. D. Miller
Massachusetts Institute of Technology

M. Brodwin
University of Missouri

S. A. Stanford
University of California, Davis

Anthony H. Gonzalez
University of Florida

See next page for additional authors

The Astrophysical Journal, 768:1 (14pp), 2013 May 1 doi:10.1088/0004-637X/768/1/1

THE CLUSTER AND FIELD GALAXY ACTIVE GALACTIC NUCLEUS FRACTION AT $z = 1$–1.5: EVIDENCE FOR A REVERSAL OF THE LOCAL ANTICORRELATION BETWEEN ENVIRONMENT AND AGN FRACTION

Paul Martini[1,2], E. D. Miller[3], M. Brodwin[4], S. A. Stanford[5,6], Anthony H. Gonzalez[7], M. Bautz[3], R. C. Hickox[8], D. Stern[9], P. R. Eisenhardt[9], A. Galametz[10], D. Norman[11], B. T. Jannuzi[12], A. Dey[11], S. Murray[13], C. Jones[13], and M. J. I. Brown[14]

[1] Department of Astronomy and Center for Cosmology and Astroparticle Physics, The Ohio State University, 140 West 18th Avenue, Columbus, OH 43210, USA; martini@astronomy.ohio-state.edu
[2] Visiting Astronomer, North American ALMA Science Center and University of Virginia, Charlottesville, VA 22903, USA
[3] Kavli Institute for Astrophysics and Space Research, Massachusetts Institute of Technology, 77 Massachusetts Avenue, Cambridge, MA 02139, USA
[4] Department of Physics and Astronomy, University of Missouri, 5110 Rockhill Road, Kansas City, MO 64110, USA
[5] Department of Physics, University of California, One Shields Avenue, Davis, CA 95616, USA
[6] Institute of Geophysics and Planetary Physics, Lawrence Livermore National Laboratory, Livermore, CA 94551, USA
[7] Department of Astronomy, University of Florida, Gainesville, FL 32611, USA
[8] Department of Physics and Astronomy, Dartmouth College, 6127 Wilder Laboratory, Hanover, NH 03755, USA
[9] Jet Propulsion Laboratory, California Institute of Technology, Pasadena, CA 91109, USA
[10] INAF-Osservatorio di Roma, Via Frascati 33, I-00040 Monteporzio, Italy
[11] NOAO, 950 North Cherry Avenue, Tucson, AZ 85719, USA
[12] Department of Astronomy and Steward Observatory, University of Arizona, 933 North Cherry Avenue, Tucson, AZ 85721, USA
[13] Harvard-Smithsonian Center for Astrophysics, 60 Garden Street, Cambridge, MA 02138, USA
[14] School of Physics, Monash University, Clayton, Victoria 3800, Australia
Received 2012 October 24; accepted 2013 February 22; published 2013 April 8

ABSTRACT

The fraction of cluster galaxies that host luminous active galactic nuclei (AGNs) is an important probe of AGN fueling processes, the cold interstellar medium at the centers of galaxies, and how tightly black holes and galaxies co-evolve. We present a new measurement of the AGN fraction in a sample of 13 clusters of galaxies ($M \geqslant 10^{14}\,M_{\odot}$) at $1 < z < 1.5$ selected from the *Spitzer*/IRAC Shallow Cluster Survey, as well as the field fraction in the immediate vicinity of these clusters, and combine these data with measurements from the literature to quantify the relative evolution of cluster and field AGN from the present to $z \sim 3$. We estimate that the cluster AGN fraction at $1 < z < 1.5$ is $f_A = 3.0^{+2.4}_{-1.4}\%$ for AGNs with a rest-frame, hard X-ray luminosity greater than $L_{X,H} \geqslant 10^{44}$ erg s^{-1}. This fraction is measured relative to all cluster galaxies more luminous than $M^*_{3.6}(z)+1$, where $M^*_{3.6}(z)$ is the absolute magnitude of the break in the galaxy luminosity function at the cluster redshift in the IRAC 3.6 μm bandpass. The cluster AGN fraction is 30 times greater than the 3σ upper limit on the value for AGNs of similar luminosity at $z \sim 0.25$, as well as more than an order of magnitude greater than the AGN fraction at $z \sim 0.75$. AGNs with $L_{X,H} \geqslant 10^{43}$ erg s^{-1} exhibit similarly pronounced evolution with redshift. In contrast to the local universe, where the luminous AGN fraction is higher in the field than in clusters, the X-ray and MIR-selected AGN fractions in the field and clusters are consistent at $1 < z < 1.5$. This is evidence that the cluster AGN population has evolved more rapidly than the field population from $z \sim 1.5$ to the present. This environment-dependent AGN evolution mimics the more rapid evolution of star-forming galaxies in clusters relative to the field.

Key words: galaxies: active – galaxies: clusters: general – galaxies: evolution – X-rays: galaxies – X-rays: galaxies: clusters – X-rays: general

Online-only material: color figures

1. INTRODUCTION

Numerous lines of evidence suggest that there is co-evolution, and perhaps a physical connection, between the growth of supermassive black holes and the formation of stars in galaxies. Perhaps the most striking result is the similar rate of evolution of the emissivity from active galactic nuclei (AGNs) and star formation from $z \sim 2$ to the present (e.g., Boyle et al. 1998; Franceschini et al. 1999; Merloni et al. 2004; Silverman et al. 2008). Presently, the correlation between the masses of supermassive black holes at the centers of galaxies and the velocity dispersions of their spheroids also supports co-evolution (e.g., Ferrarese & Merritt 2000; Gebhardt et al. 2000; Tremaine et al. 2002) and may indicate a causal connection. Other evidence for a connection between black holes and galaxy growth includes that AGNs are much more common in the most luminous starburst galaxies (e.g., Sanders et al. 1988; Veilleux et al. 2009) and that even low-luminosity AGNs are more commonly found in galaxies with some young stellar populations compared to otherwise similar inactive galaxies (e.g., Terlevich et al. 1990; Kauffmann et al. 2003).

These observational correlations have fueled a lot of investigation into the processes that drive matter to accrete onto supermassive black holes, as well as form new stars. The prevalent theoretical framework is that the most luminous AGNs and starbursts are triggered by major mergers of gas-rich galaxies (e.g., Sanders et al. 1988; Barnes & Hernquist 1991; Hopkins et al. 2006). Numerous other mechanisms have also been proposed to remove angular momentum and fuel star formation and black hole growth at lower rates, such as large-scale bars, other weakly nonaxisymmetric variations in the gravitational potential, minor mergers, disk instabilities, and turbulence in the interstellar medium (ISM) (e.g., Simkin et al. 1980; Elmegreen et al. 1998; Genzel et al. 2008; Hopkins & Quataert 2011). The

observational connection between these mechanisms and lower-luminosity AGNs is less clear (e.g., Fuentes-Williams & Stocke 1988; Mulchaey & Regan 1997; Martini et al. 2003), most likely because there are progressively more ways to fuel progressively smaller amounts of star formation and black hole growth (see Martini 2004 for a review).

The distribution of AGNs in clusters of galaxies relative to the field provides some valuable additional observational constraints on fueling processes as a function of luminosity or accretion rate, as well as the connection between black hole and galaxy growth. This is because additional physical processes impact the availability and transport of the cold gas that serves as the primary fuel source for the central black hole. These processes include the removal of cold gas via ram-pressure stripping (Gunn & Gott 1972), evaporation by the hot ISM (Cowie & Songaila 1977), tidal effects due to the cluster potential (Farouki & Shapiro 1981; Merritt 1983) and other galaxies (Richstone 1976; Moore et al. 1996), and gas starvation due to the absence of new infall of cold gas (Larson et al. 1980). These physical processes have been invoked to explain the relative absence of luminous, star-forming galaxies in clusters, the scarcity of substantial reservoirs of cold gas, and the large fraction of relatively quiescent, early-type galaxies (Gisler 1978; Dressler 1980; Giovanelli & Haynes 1985; Dressler et al. 1999). Observational studies of AGNs in local clusters have similarly found that luminous AGNs are rarer in cluster galaxies compared to field galaxies (Kauffmann et al. 2004; Popesso & Biviano 2006), although less-luminous AGNs appear to be present in comparable numbers (Martini et al. 2002; Miller et al. 2003; Best et al. 2005a; Martini et al. 2006; Haggard et al. 2010).

The different, or at least additional, physical processes that influence galaxy evolution in clusters make the cluster environment very well suited to study the co-evolution of supermassive black holes and galaxies. This is because the formation and evolution of galaxies has proceeded at a different rate in clusters relative to the field. For example, the stars in cluster galaxies appear to have an earlier mean formation epoch than field galaxies of similar mass (e.g., van Dokkum & Franx 1996; Kelson et al. 1997). Star formation in cluster galaxies is also observed to increase rapidly with redshift (Butcher & Oemler 1978; Saintonge et al. 2008; Haines et al. 2009; Hilton et al. 2010; Tran et al. 2010; Atlee & Martini 2012). If the evolution of AGNs in clusters traces the evolution of star-forming galaxies in clusters, rather than the evolution of star-forming galaxies and AGNs in the field, this will be strong evidence that AGNs and star formation are physically connected, and not just a cosmic coincidence.

The first evidence that substantial numbers of AGNs may be present in higher-redshift clusters came from the discovery of three AGNs in the $z = 0.46$ cluster 3C295 by Dressler & Gunn (1983), although subsequent spectroscopic surveys of other clusters at similar redshifts did not find AGNs in large numbers (Dressler et al. 1985). Later *Chandra* observations of many $z > 0.5$ clusters did find evidence for AGNs through the detection of higher surface densities of X-ray point sources in the fields of these clusters (Cappelluti et al. 2005; Gilmour et al. 2009), although spectroscopic follow-up observations were only obtained in a few cases (Johnson et al. 2003; Demarco et al. 2005). The first quantitative evidence for a substantial increase in the cluster AGN fraction with redshift was presented by Eastman et al. (2007) who compared the fraction of spectroscopically confirmed AGNs of similar X-ray luminosities in low- and high-redshift clusters. A larger study by Galametz et al. (2009) further quantified the increase in the AGN fraction based on surface density measurements of X-ray, MIR, and radio AGNs. Martini et al. (2009) used a spectroscopically confirmed sample to demonstrate that the AGN fraction f_A increases as $(1+z)^{5.3}$ for AGNs above a hard X-ray luminosity of $L_X \geqslant 10^{43}$ erg s^{-1} hosted by galaxies more luminous than $M_R^*(z)+1$, where $M_R^*(z)$ is the absolute magnitude of the knee of the galaxy luminosity function at redshift z. This study included a total of 32 clusters from the local universe to $z \sim 1.3$ and included data from many previous cluster studies (Martini et al. 2006; Eckart et al. 2006; Martini et al. 2007; Sivakoff et al. 2008). Several more recent studies have also identified AGNs in high-redshift clusters and groups (Rumbaugh et al. 2012; Fassbender et al. 2012; Tanaka et al. 2012). The rapid rate of AGN evolution is quite similar to the evolution of the fraction of star-forming galaxies in clusters of $f_{\rm SF} \propto (1+z)^{5.7}$ reported by Haines et al. (2009), and suggests the AGN and star-forming galaxy populations evolve at similar rates in clusters, although both power-law indices are uncertain by approximately ± 2.

The evolution of the AGN fraction in clusters of galaxies quantified by Martini et al. (2009) appears to be substantially greater than the evolution of the AGN fraction in the field. Work by Alonso-Herrero et al. (2008) and Bundy et al. (2008) demonstrated that the AGN fraction increases by only about a factor of two from $z \sim 0.5$ to $z \sim 1.2$, which is several times smaller than the increase for cluster AGNs. This relative evolution appears broadly consistent with the behavior of star-forming galaxies over the same redshift range. Elbaz et al. (2007) showed that the fraction of galaxies that are star forming is correlated with local galaxy density at $z \sim 1$, which is a reversal of the anticorrelation observed in the local universe. Nevertheless, a direct comparison between field and cluster surveys is complicated because they often employ different selection criteria, such as luminosity in some band, or an estimate of the stellar mass, and different AGN luminosity limits, to establish their host galaxy and AGN samples. These selection criteria are important because the AGN fraction above a given luminosity limit depends on stellar mass (e.g., Heckman et al. 2004; Sivakoff et al. 2008; Aird et al. 2012) and the evolution of the X-ray luminosity function indicates that more luminous AGNs were proportionally more abundant at higher redshift (Hasinger et al. 2005; Barger et al. 2005), a phenomenon known as "AGN downsizing."

In this paper, we present a new study of a homogenous sample of clusters of galaxies at the crucial redshift range of $1 < z < 1.5$ where earlier work implied that the fraction of cluster and field AGNs would be substantially more similar than they are at the present day. These clusters were selected from the *Spitzer*/IRAC Shallow Cluster Survey (ISCS; Eisenhardt et al. 2008), and have uniform visible, near-infrared, and *Spitzer* observations, deep *Chandra* observations to identify luminous AGNs, and substantial photometric and spectroscopic redshift data. We describe these data sets further in the next section. We use these data to uniformly select AGNs with X-ray and MIR criteria, as described in Section 3, and compare the AGN fraction in the clusters with the immediate field environment in Section 4 to demonstrate the similarity of the field and cluster AGN fractions in this redshift range. In Section 5 we calculate the cluster AGN fraction for this sample and compare it to lower-redshift clusters, then in Section 6 we discuss the relative evolution of the field and cluster AGN fraction from the present day to $z \sim 3$. We adopt $(\Omega_M, \Omega_\Lambda, h) = (0.3, 0.7, 0.7)$ for the cosmological parameters.

Table 1
Properties of the High-redshift Clusters

Cluster	α	δ	z	ObsID	$t_{\rm exp}$ (ks)	$M^*_{3.6\,\mu{\rm m}}$ (mag)
(1)	(2)	(3)	(4)	(5)	(6)	(7)
ISCSJ1429.2+3357	14:29:15.2	33:57:08.5	1.06	10450	23	17.20
ISCSJ1432.4+3332	14:32:29.2	33:32:36.0	1.11	10452	34	17.25
ISCSJ1426.1+3403	14:26:09.5	34:03:41.1	1.14	10451, 7945, 6995	11, 41, 10	17.30
ISCSJ1426.5+3339	14:26:30.4	33:39:33.2	1.16	10453	35	17.30
ISCSJ1434.5+3427	14:34:30.4	34:27:12.3	1.24	10455	34	17.50
ISCSJ1429.3+3437	14:29:18.5	34:37:25.8	1.26	10454	30	17.50
ISCSJ1432.6+3436	14:32:38.4	34:36:49.0	1.35	10456	32	17.60
ISCSJ1425.3+3428	14:25:19.3	34:28:38.2	1.36	10458	36	17.60
ISCSJ1433.8+3325	14:33:51.1	33:25:51.1	1.37	7946	40	17.60
ISCSJ1434.7+3519	14:34:46.3	35:19:33.5	1.37	10459	32	17.60
ISCSJ1432.3+3253	14:32:18.3	32:53:07.8	1.40	10457	34	17.65
ISCSJ1438.1+3414	14:38:08.7	34:14:19.2	1.41	10461	101(s)	17.65
ISCSJ1432.4+3250	14:32:24.2	32:50:03.7	1.49	10457	34	17.75

Notes. Properties of the clusters in the sample. Columns are: (1) cluster name; (2) and (3) right ascension and declination (J2000) of the cluster center; (4) redshift; (5) *Chandra* ObsID of the data set(s) used in the analysis; (6) total integration time of the *Chandra* data; and (7) Vega magnitude at 3.6 μm of L^* at the cluster redshift from Eisenhardt et al. (2008). Clusters were observed with the *Chandra* ACIS-I camera with the exception of ISCSJ1438.1+3414 (ACIS-S).

2. DESCRIPTION OF THE DATA

Our parent cluster sample was selected from the IRAC Shallow Survey described by Eisenhardt et al. (2004). This survey covers 8.5 deg^2 in the NOAO Deep Wide-Field Survey in Boötes (NDWFS; Jannuzi & Dey 1999) with at least 90 s of integration time in each of the four IRAC bands. These data were supplemented with additional photometry from the *Spitzer* Deep, Wide-Field Survey (Ashby et al. 2009), which added nine more 30 s exposures across the entire area with IRAC. Deep B_W-, R-, and I-band data from the Mosaic-1 camera on the KPNO 4 m telescope were obtained for the NDWFS. Near-infrared images from the FLAMINGOS Extragalactic Survey are also available for half of the field (Elston et al. 2006). Deeper, near-infrared data have more recently been obtained for the entire field with NEWFIRM (A. H. Gonzalez et al., in preparation).

The photometric data were used by Brodwin et al. (2006) to calculate photometric redshifts and redshift probability distribution functions $P(z)$ with an empirical template-fitting algorithm. The large AGN and Galaxy Evolution Survey (Kochanek et al. 2012) of the Boötes field, together with other spectroscopic redshift surveys in this region, was used to create training sets and improve the accuracy of the photometric redshifts. Based on over 15,000 galaxies with spectroscopic redshifts, these photometric redshifts have an uncertainty of $\sigma_z = 0.06(1+z)$ for $0 < z < 1.5$. The photometric redshift calculations are described in detail in Brodwin et al. (2006).

Eisenhardt et al. (2008) employed a wavelet analysis technique to identify galaxy clusters within the Boötes field for the ISCS. The photometric redshift distributions $P(z)$ were used to construct weighted galaxy density maps as a function of redshift. These density maps in redshift space were then convolved with a wavelet kernel and galaxy cluster candidates were identified as peaks in the wavelet-smoothed density maps. The significance level for each redshift slice was determined with bootstrap resamples of the positions and $P(z)$ distributions for the galaxies. Eisenhardt et al. (2008) identified a total of 106 cluster candidates at $z > 1$ with this technique and estimated that only ~10% may be due to chance or projection effects. A number of these clusters have been spectroscopically confirmed to date (Stanford et al. 2005; Brodwin et al. 2006, 2011; Elston et al. 2006; Eisenhardt et al. 2008; Zeimann et al. 2012; M. Brodwin et al., in preparation), where spectroscopic confirmation is defined to mean that at least five galaxies have redshifts within $\pm 2000(1+z_{\rm spec})$ km s^{-1} of the average spectroscopic redshift $z_{\rm spec}$ and lie within $R < 2$ Mpc of the cluster center.

Our study focuses on 13 clusters that were among the most significant from Eisenhardt et al. (2008). Of these clusters, 11 were targeted as part of a *Chandra* GO program in 2009 to obtain exposures of 30–40 ks (they were also included in the larger XBoötes survey; Murray et al. 2005; Kenter et al. 2005). The remaining two clusters have archival data with sufficient exposures to include in this study. Two other cluster candidates identified by Eisenhardt et al. (2008) also have similar X-ray data, although they are not included in this analysis. These two clusters are ISCSJ1427.9+3430, which is likely a superposition of ~4 groups along the line of sight, and ISCSJ1429.2+3425, which appears to be a close pair of clusters. We do not include ISCSJ1427.9+3430 in our analysis because it is unlikely to be a massive cluster. We do not include ISCSJ1429.2+3425 because the proximity of the cluster pair would add uncertainty to our estimate of foreground and background contamination. Table 1 lists the basic properties of the 13 clusters, as well as the data sets that we use for this study. All of the clusters were observed with the ACIS-I camera, with the exception of ISCSJ1438.1+3414, which was observed with ACIS-S. The field of view of these observations was $16\farcm8 \times 16\farcm8$ (ACIS-I) or $8\farcm4 \times 8\farcm4$ (ACIS-S). In all cases the cluster was approximately centered in the field of view. This field of view is adequate to encompass the entire angular extent of these clusters out to approximately the r_{200} radius, the radius within which the cluster is a factor of 200 overdense relative to the average field value, with the exception of some area lost to gaps between the ACIS-I chips. These data also include substantial coverage out to larger radii, which we use to estimate the field population at the cluster redshift.

We estimated the approximate masses and sizes of these clusters in several ways. First, Brodwin et al. (2007) measured the autocorrelation function of ISCS clusters and found $r_0 = 19.14^{+5.65}_{-4.56}\ h^{-1}$Mpc at $z = 1$, which corresponds to a mean cluster mass of $\sim 10^{14}\ M_\odot$. Based on Carlberg et al. (1997), we estimate that the typical r_{200} radius of these clusters is ~1 Mpc, which corresponds to ~2′ at the typical redshift of these clusters.

This mean cluster mass estimate, and thus the inferred size, has been confirmed with more detailed studies of individual clusters. Brodwin et al. (2011) studied ISCSJ1438.1+3414 ($z = 1.414$) and ISCSJ1432.4+3250 ($z = 1.487$) with deep *Chandra* observations and extensive spectroscopic observations. This study showed that ISCSJ1438.1+3414 has a velocity dispersion of 747^{+247}_{-208} km s^{-1} based on 17 members, which corresponds to a dynamical mass of $\log M_{200,\rm dyn} = 14.5^{+0.3}_{-0.7}$ in solar masses. The dynamical mass estimate is in very good agreement with the estimate of $\log M_{200,X} = 14.35^{+0.11}_{-0.14}$ in solar masses from the cluster's X-ray luminosity. While there is no dynamical mass estimate for the higher-redshift ISCSJ1432.4+3250 cluster, the mass estimated from the X-ray luminosity is similar: $\log M_{200,X} = 14.4 \pm 0.2$ in solar masses. Many of these clusters were also included in the weak-lensing study by Jee et al. (2011) and these mass estimates are all above $10^{14}\ M_{\odot}$. As we do not have individual mass estimates for all 13 clusters, but do know they are similar based on their selection, we adopt a projected radius of 2′ for all the clusters.

There are typically 5–15 spectroscopically confirmed members in each cluster. Because the spectroscopic data are not complete, we supplement these data with cluster members based on photometric redshifts for some of our analysis. We identify these members based on the integral of $P(z)$ from $z - 0.06(1 + z)$ to $z + 0.06(1 + z)$, where z is the cluster redshift. Galaxies are identified as cluster members if at least 30% of the redshift probability distribution is within this range and their position is within a projected separation of 2′ of the cluster center. This photometric redshift criterion will include foreground and background galaxies. We use a sample of galaxies that satisfy the same photometric redshift criterion, but are projected to lie from 2′ up to 10′ radius (a physical size of r_{200} to $5r_{200}$), to define a field sample and estimate the foreground and background contamination. Many studies have found evidence that clusters may impact the surrounding field or "infall" region galaxy population at distances up to $5r_{200}$ (e.g., Patel et al. 2009; Balogh et al. 2009). While we estimate the field contamination from this region rather than the true field, our results below indicate that this distinction is unimportant for our analysis. This is likely because galaxies that have already been affected by the cluster do not dominate the surface density of galaxies that satisfy the photometric redshift criterion. We also only include galaxies that are no fainter than one magnitude below the knee of the luminosity function, $M^*_{3.6} + 1$ at the cluster redshift. The break in the luminosity function for clusters over this redshift range was calculated by Mancone et al. (2010). The apparent magnitude that corresponds to the break in the luminosity function at the redshift of each cluster is listed in Table 1. Figure 1 shows a color–magnitude diagram for each cluster, where larger symbols refer to membership based on spectroscopic redshifts and smaller symbols to photometric redshifts. The apparent magnitudes that correspond to $M^*_{3.6}$ and $M^*_{3.6} + 1$ for each cluster are also shown on each panel.

3. AGN IDENTIFICATION

AGNs in high-redshift clusters have previously been selected based on radio emission (Johnson et al. 2003; Galametz et al. 2009; Gralla et al. 2011) and X-ray emission (Johnson et al. 2003; Eastman et al. 2007; Galametz et al. 2009; Martini et al. 2009). These techniques have unambiguously determined that luminous AGNs are present in high-redshift clusters because only black hole accretion can produce such luminous emission at these redshifts. In the first subsection below, we describe how we process and then analyze our X-ray observations to identify X-ray AGNs in clusters and the field and characterize their properties. MIR selection based on IRAC color selection (Lacy et al. 2004; Stern et al. 2005; Assef et al. 2010; Donley et al. 2012) can also effectively identify AGNs at these redshifts due to the very different spectral energy distribution (SED) shape of AGNs relative to normal and star-forming galaxies. This is described further in the following subsection.

3.1. X-Ray AGNs

The *Chandra* data were reprocessed with CIAO v4.3 and calibration products from CALDB v4.4.1. Point sources were identified from a full-resolution image in the observed 0.5–7 keV energy range using `wavdetect`, a wavelet source detection tool available in CIAO. We searched at wavelet scales between 1 and 32 pixels (0.492 and 15.7 arcsec) to detect a range of source sizes and to account for the variable point-spread function (PSF) across the ACIS field. A `wavdetect` threshold of 10^{-6} was chosen, which corresponds to the likelihood of incorrectly detecting a source at a given pixel. For the ACIS-I observations, only the four ACIS-I detectors were included in the search, therefore we expect about four spurious detections in each 2048×2048 pixel field. One of the clusters (ISCSJ1438.1+3414) was observed with ACIS-S centered on the S3 detector; we used the same `wavdetect` parameters for this observation, only including the single detector. Detections of greater than four net counts were kept in the intermediate source lists, which resulted in 70 candidate detections of greater than 2σ confidence in a typical 35 ks observation.

One cluster (ISCSJ1426.1+3403) has a substantially shorter on-axis *Chandra* exposure (11 ks). To validate the `wavdetect` results, which were only performed for the on-axis observation, we included two additional archival data sets, OBSID 7945 (40 ks) and 6995 (10 ks). These observations were taken with the cluster very close to the edge of the field of view, but in opposite directions north and south. We used acis_extract (Broos et al. 2010), which searches for sources in multiple overlapping observations and accounts for non-uniform exposures and PSF sizes in the searched region. This procedure resulted in no additional point-source detections within 4′ of the cluster center.

We cross-correlated our cluster member catalogs and the X-ray point-source catalogs and identified all cluster members with an X-ray source within 2″ of the IRAC position. Eleven of the cluster galaxies brighter than $M^*_{3.6} + 1$ are associated with significant X-ray emission. The coordinates, redshifts, and apparent magnitudes of these galaxies are listed in Table 2.

We calculated the flux and luminosity of each X-ray source in various observed and rest-frame bands with a $\Gamma = 1.7$ power-law model, after a correction for Galactic absorption. The counts, significance, observed-frame 0.5–8 and 2–8 keV fluxes, and rest-frame 0.5–8 and 2–10 keV luminosities are provided in Table 3. All of these X-ray sources have rest-frame, 2–10 keV luminosities greater than $L_{X,H} > 10^{43}$ erg s^{-1}. Only AGNs are known to produce point-source emission at these luminosities and we consequently classify all these galaxies as X-ray AGNs. Of the 11 X-ray AGNs, 8 have spectroscopic redshifts that confirm they are cluster members, including all 4 with $L_{X,H} > 10^{44}$ erg s^{-1}. The presence of X-ray emission was not used as a selection criterion to target candidate cluster members for spectroscopy; however, two of the spectroscopically confirmed AGNs were selected based on their MIR colors, as described in the next subsection.

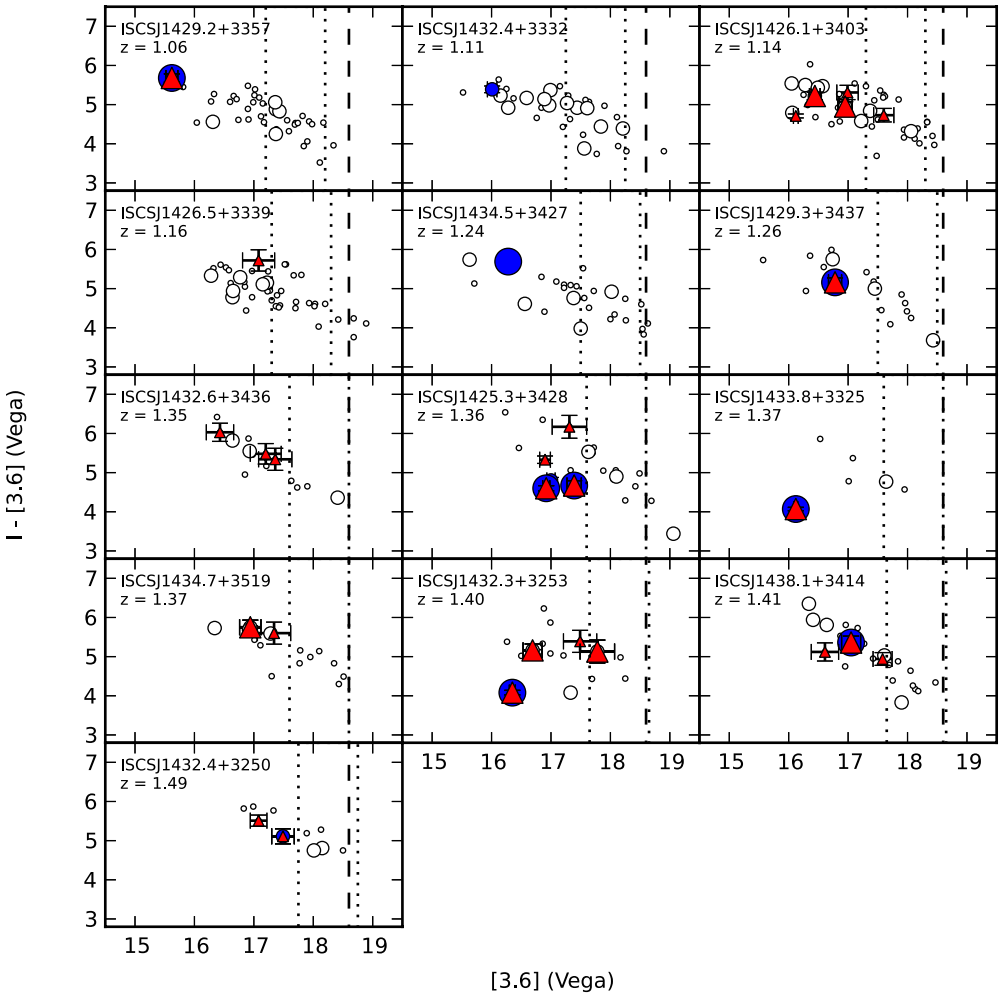

Figure 1. Color–magnitude diagrams for cluster members based on spectroscopic (large symbols) or photometric (small symbols) redshifts. All cluster members that have photometric uncertainties less than 0.3 mag in the I and 3.6 μm bands and lie within 2′ of the cluster center are shown. Error bars are only shown for X-ray AGNs (blue circles) and MIR AGNs (red triangles). The vertical, dotted lines correspond to the apparent magnitudes of $M^*_{3.6}$ and $M^*_{3.6}+1$ at the cluster redshift. Only cluster members more luminous than $M^*_{3.6}+1$ are employed in our analysis. The vertical, dashed line represents the [3.6] mag that corresponds to a red galaxy at the [4.5] = 17.8 mag limit employed by Eisenhardt et al. (2008).

(A color version of this figure is available in the online journal.)

Our X-ray data do not have uniform depth over the area subtended by each cluster and field region. The non-uniformity is due to the gaps between the ACIS-I detectors and how well the clusters were centered on the detectors. We used exposure maps for each cluster to quantify the fraction of the cluster and field area with sufficient depth to identify AGNs. We identified a sensitivity threshold for each exposure map that corresponds to an AGN with a rest-frame 2–10 keV luminosity of 10^{44} erg s^{-1} at the cluster redshift. The fraction of the cluster and field regions above this threshold for each cluster is used to quantify the X-ray AGN surface density and X-ray AGN fraction in the following sections.

3.2. MIR AGNs

We used our IRAC data to identify candidate cluster AGNs with the MIR color-selection criteria defined by Stern et al. (2005) and refer to these as MIR AGNs. Color–color diagrams for the clusters are shown in Figure 2. Galaxies were only classified if the photometric uncertainties were less than 0.3 mag in all four IRAC bands. There are 27 MIR AGNs, of which 12 have spectroscopic redshifts. Of the 11 X-ray AGNs, 8 were also identified as MIR AGNs, including all the X-ray AGNs more luminous than $L_{X,H} \geqslant 10^{44}$ erg s^{-1}. The incomplete overlap between the MIR AGNs and the X-ray AGNs is consistent with previous studies, which have found similar results for the field (Hickox et al. 2009) and in low-redshift clusters (Atlee et al. 2011). Unlike the case for X-ray AGNs, J142916.1+335537 in ISCSJ1429.2+3357 and J143816.8+341440 in ISCSJ1438.1+3414 were selected for spectroscopic observations as cluster MIR AGN candidates. Both of these MIR AGNs are also X-ray AGNs.

4. RADIAL DISTRIBUTIONS

The projected distribution of all galaxies consistent with each cluster's redshift, including the X-ray and MIR AGNs, is shown in Figure 3. The adopted angular size for each of the clusters is 2′, which is approximately the value of r_{200} (∼1 Mpc) at the redshift of these clusters (see Section 2). Field galaxies consistent with the cluster redshift are shown within an 8′ × 8′ box centered on each cluster to illustrate the environment in the immediate vicinity of these clusters. We use these galaxies, including AGNs, from $R = 2' \rightarrow 10'$ to measure the surface density of field galaxies and quantify the amount of foreground

Table 2
AGNs in the High-Redshift Clusters

ID (1)	Cluster (2)	Redshift (3)	α (4)	δ (5)	I (6)	[3.6] (7)	X/IR (8)
J142916.1+335537	ISCSJ1429.2+3357	1.06^{s}	14:29:16.1	+33:55:37.3	21.30 (0.10)	15.62 (0.03)	Both
J143227.2+333307	ISCSJ1432.4+3332	1.15^{p}	14:32:27.2	+33:33:07.5	21.40 (0.08)	16.01 (0.03)	X-ray
J142611.6+340226	ISCSJ1426.1+3403	1.14^{s}	14:26:11.6	+34:02:26.0	21.90 (0.12)	16.95 (0.03)	IR
J142607.6+340309	ISCSJ1426.1+3403	1.12^{s}	14:26:07.6	+34:03:09.3	21.66 (0.09)	16.44 (0.03)	IR
J142602.8+340405	ISCSJ1426.1+3403	1.26^{p}	14:26:02.8	+34:04:05.8	22.30 (0.18)	16.99 (0.03)	IR
J142610.2+340355	ISCSJ1426.1+3403	1.10^{p}	14:26:10.2	+34:03:55.6	22.33 (0.17)	17.60 (0.03)	IR
J142608.3+340430	ISCSJ1426.1+3403	1.09^{p}	14:26:08.3	+34:04:30.0	20.83 (0.04)	16.12 (0.03)	IR
J142627.5+333912	ISCSJ1426.5+3339	1.28^{p}	14:26:27.5	+33:39:12.8	22.80 (0.27)	17.08 (0.03)	IR
J143430.3+342712	ISCSJ1434.5+3427	1.24^{s}	14:34:30.3	+34:27:12.0	21.97 (0.14)	16.28 (0.03)	X-ray
J142915.2+343709	ISCSJ1429.3+3437	1.27^{s}	14:29:15.2	+34:37:09.2	21.94 (0.11)	16.78 (0.03)	Both
J143232.7+343538	ISCSJ1432.6+3436	1.22^{p}	14:32:32.7	+34:35:38.4	22.70 (0.28)	17.36 (0.03)	IR
J143237.8+343630	ISCSJ1432.6+3436	1.31^{p}	14:32:37.8	+34:36:30.9	22.46 (0.23)	16.43 (0.03)	IR
J143238.8+343647	ISCSJ1432.6+3436	1.28^{p}	14:32:38.8	+34:36:47.6	22.68 (0.26)	17.20 (0.03)	IR
J142512.9+342735	ISCSJ1425.3+3428	1.21^{p}	14:25:12.9	+34:27:35.2	21.80 (0.07)	17.00 (0.03)	X-ray
J142516.5+342755	ISCSJ1425.3+3428	1.36^{s}	14:25:16.5	+34:27:55.7	22.06 (0.12)	17.39 (0.03)	Both
J142520.3+342942	ISCSJ1425.3+3428	1.36^{s}	14:25:20.3	+34:29:42.8	21.52 (0.06)	16.92 (0.03)	Both
J142520.2+343014	ISCSJ1425.3+3428	1.36^{p}	14:25:20.2	+34:30:14.3	23.48 (0.29)	17.31 (0.03)	IR
J142519.8+343024	ISCSJ1425.3+3428	1.17^{p}	14:25:19.8	+34:30:24.8	22.23 (0.09)	16.90 (0.03)	IR
J143351.5+332645	ISCSJ1433.8+3325	1.37^{s}	14:33:51.5	+33:26:45.8	20.19 (0.03)	16.12 (0.03)	Both
J143445.7+351921	ISCSJ1434.7+3519	1.37^{s}	14:34:45.7	+35:19:21.7	22.69 (0.18)	16.94 (0.03)	IR
J143450.0+351958	ISCSJ1434.7+3519	1.43^{p}	14:34:50.0	+35:19:58.8	22.94 (0.28)	17.34 (0.03)	IR
J143216.4+325434	ISCSJ1432.3+3253	1.39^{s}	14:32:16.4	+32:54:34.1	20.43 (0.05)	16.35 (0.03)	Both
J143216.4+325224	ISCSJ1432.3+3253	1.41^{s}	14:32:16.4	+32:52:24.9	22.91 (0.29)	17.78 (0.04)	IR
J143217.1+325235	ISCSJ1432.3+3253	1.27^{p}	14:32:17.1	+32:52:35.1	22.88 (0.28)	17.49 (0.03)	IR
J143218.1+325315	ISCSJ1432.3+3253	1.40^{s}	14:32:18.1	+32:53:15.9	21.85 (0.16)	16.69 (0.03)	IR
J143816.8+341440	ISCSJ1438.1+3414	1.41^{s}	14:38:16.8	+34:14:40.3	22.41 (0.16)	17.05 (0.03)	Both
J143817.4+341337	ISCSJ1438.1+3414	1.46^{p}	14:38:17.4	+34:13:37.6	22.52 (0.16)	17.58 (0.03)	IR
J143802.7+341548	ISCSJ1438.1+3414	1.42^{p}	14:38:02.7	+34:15:48.2	21.73 (0.23)	16.61 (0.03)	IR
J143217.1+325055	ISCSJ1432.4+3250	1.58^{p}	14:32:17.1	+32:50:55.1	22.60 (0.19)	17.49 (0.03)	Both
J143224.8+325005	ISCSJ1432.4+3250	1.31^{p}	14:32:24.8	+32:50:05.0	22.59 (0.14)	17.08 (0.03)	IR

Notes. AGNs in the high-redshift clusters. Columns are: (1) AGN ID; (2) cluster name; (3) AGN redshift, either photometric (*p*) or spectroscopic (*s*); (4) and (5) right ascension and declination (J2000); (6) and (7) *I* and [3.6] (Vega) mag; and (8) AGN selection via X-ray, IR, or both criteria. For AGNs with photometric redshifts, the redshift listed in Column 3 may not agree with the cluster redshift because it corresponds to the peak of the redshift probability distribution function, while membership is based on the fraction of the integrated probability at the cluster redshift. See Section 2 for further details.

Table 3
X-Ray Properties of the Cluster AGN

ID (1)	Cluster (2)	Redshift (3)	Counts (4)	Sig (5)	$F_{0.5-8}$ (6)	F_{2-8} (7)	$L_{0.5-8}$ (8)	L_{2-10} (9)
J142916.1+335537	ISCSJ1429.2+3357	1.06^{s}	89	44.0	6.71 (0.70)	4.04 (0.42)	3.20 (0.33)	2.44 (0.26)
J143227.2+333307	ISCSJ1432.4+3332	1.15^{p}	6	3.5	0.25 (0.09)	0.15 (0.06)	0.14 (0.05)	0.11 (0.04)
J143430.3+342712	ISCSJ1434.5+3427	1.24^{s}	11	6.0	0.49 (0.13)	0.29 (0.08)	0.33 (0.09)	0.26 (0.07)
J142915.2+343709	ISCSJ1429.3+3437	1.27^{s}	75	37.0	4.11 (0.47)	2.48 (0.28)	2.91 (0.33)	2.28 (0.26)
J142512.9+342735	ISCSJ1425.3+3428	1.21^{p}	4	2.4	0.20 (0.08)	0.12 (0.05)	0.12 (0.05)	0.10 (0.04)
J142516.5+342755	ISCSJ1425.3+3428	1.36^{s}	25	12.8	0.99 (0.18)	0.59 (0.11)	0.81 (0.15)	0.65 (0.12)
J142520.3+342942	ISCSJ1425.3+3428	1.36^{s}	25	12.4	0.90 (0.17)	0.54 (0.10)	0.72 (0.17)	0.58 (0.14)
J143351.5+332645	ISCSJ1433.8+3325	1.37^{s}	81	39.1	2.65 (0.28)	1.60 (0.17)	2.21 (0.24)	1.76 (0.19)
J143216.4+325434	ISCSJ1432.3+3253	1.39^{s}	63	25.9	2.55 (0.31)	1.54 (0.19)	2.21 (0.27)	1.75 (0.21)
J143816.8+341440	ISCSJ1438.1+3414	1.41^{s}	10	4.5	0.30 (0.05)	0.18 (0.03)	0.26 (0.04)	0.21 (0.03)
J143217.1+325055	ISCSJ1432.4+3250	1.58^{p}	9	5.0	0.43 (0.14)	0.26 (0.08)	0.49 (0.15)	0.40 (0.13)

Notes. X-ray properties of the AGNs in the high-redshift clusters. Columns are: (1) AGN ID; (2) cluster name; (3) AGN redshift, either photometric (*p*) or spectroscopic (*s*); (4) counts; (5) significance of the X-ray detection; (6) and (7) unabsorbed flux in the observed-frame 0.5–8 keV and 2–8 keV bands in units of 10^{-14} erg cm^{-2} s^{-1}; (8) and (9) unabsorbed luminosity in the rest-frame 0.5–8 keV and 2–10 keV bands in units of 10^{44} erg s^{-1}.

and background contamination in the cluster sample. A fraction of the cluster and field area does not have complete X-ray coverage due to chip gaps and the exact placement of the cluster center relative to the center of the ACIS field of view. We correct for the non-uniform X-ray coverage as described in Section 3.1.

As luminous AGNs are too rare to study their distribution within individual clusters, we stack the cluster catalogs to measure their radial distribution. The total number of sources per 0.′5 bin as a function of distance from the cluster center is shown in Figure 4. The solid lines correspond to all galaxies that are at the cluster redshift. The dotted lines only include galaxies with spectroscopic redshifts. The almost complete lack of galaxies with spectroscopy outside of 2′ is because these galaxies were generally not spectroscopic targets. Because the spectroscopic

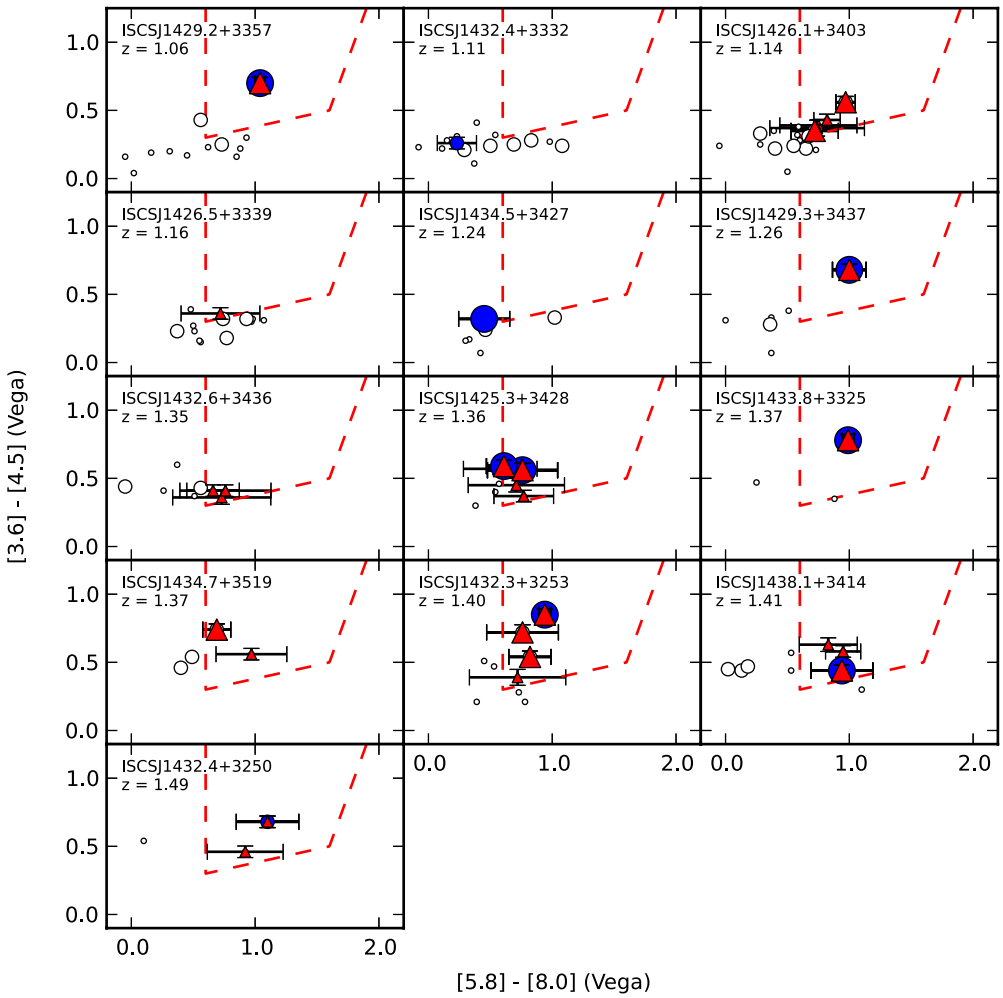

Figure 2. IRAC color–color plots for members of the clusters listed in Table 1 (all points). Error bars are only shown for X-ray AGNs (blue circles) and MIR AGNs (red triangles). Large symbols correspond to spectroscopically confirmed cluster members. Small symbols correspond to photometric redshifts. Galaxies are only shown if they are projected to lie within 2′ of the cluster center, have photometric uncertainties less than 0.3 mag in all four IRAC bands, and they are brighter than $M^*_{3.6}(z) + 1$, where $M^*_{3.6}(z)$ is the [3.6] mag of the break in the luminosity function at the cluster redshift.

(A color version of this figure is available in the online journal.)

coverage is fairly high in the clusters, we only use AGNs with spectroscopic redshifts to compare to AGNs in clusters at other redshifts. We use photometric redshifts to estimate the total number of cluster galaxies, as well as to estimate the relative AGN fractions of X-ray and MIR AGNs in clusters and the field.

Figure 5 shows the surface density of all galaxies (left), and X-ray and MIR AGNs (right). The surface densities for all galaxies and for MIR AGNs are simply the raw counts shown in Figure 4 divided by the total area of each annulus. The surface density of X-ray AGNs is computed from the total area in each radial bin that is above the fixed luminosity sensitivity threshold described in Section 2. The surface density of galaxies, X-ray AGNs, and MIR AGNs all asymptote to constant values by approximately 2′ from the cluster center, which is consistent with the adopted radius of 2′ for these clusters. We estimate that small uncertainties in our choice of 2′ for the radius of these clusters will not impact our results.

We use the data from 2′ → 10′ to estimate the field surface density of all galaxies and MIR AGNs, while we use the data from 2′ → 6′ for all galaxies that have X-ray coverage and X-ray AGNs. The radial range for the X-ray coverage is smaller because of the size of the X-ray images and the deterioration of the PSF further off axis. The surface densities for all galaxies, all galaxies with X-ray coverage, X-ray AGNs, and MIR AGNs are 0.90, 0.99, 0.04, and 0.07 arcmin^{-2}, respectively. We use the field density to calculate the foreground and background contamination within the clusters, and then calculate and subtract an estimate of the contamination from the total number of galaxies within a projected radius of $R = 2'$ to estimate the total number of cluster members, X-ray AGNs, and MIR AGNs in the cluster sample. In the case of X-ray AGNs, this includes a correction that accounts for the fact that not all the projected cluster and field area is above the X-ray luminosity threshold. We estimate that there are a total of 150 galaxies in these 13 clusters above the galaxy luminosity threshold and 136 of these galaxies lie within the area above our X-ray luminosity threshold. This surface density extrapolation also leads to an expectation of 5 X-ray AGNs and 15 MIR AGNs in these clusters. These values are consistent with the 8 and 12 spectroscopically confirmed X-ray and MIR AGNs in these clusters (8 AGNs are common to both samples) listed in Tables 2 and 3.

The fractional surface densities of X-ray and MIR AGNs in the cluster and field samples are consistent with one another. The X-ray and MIR AGN fractions in the clusters and the field are shown in Figure 6. Note that these fractions do not correspond

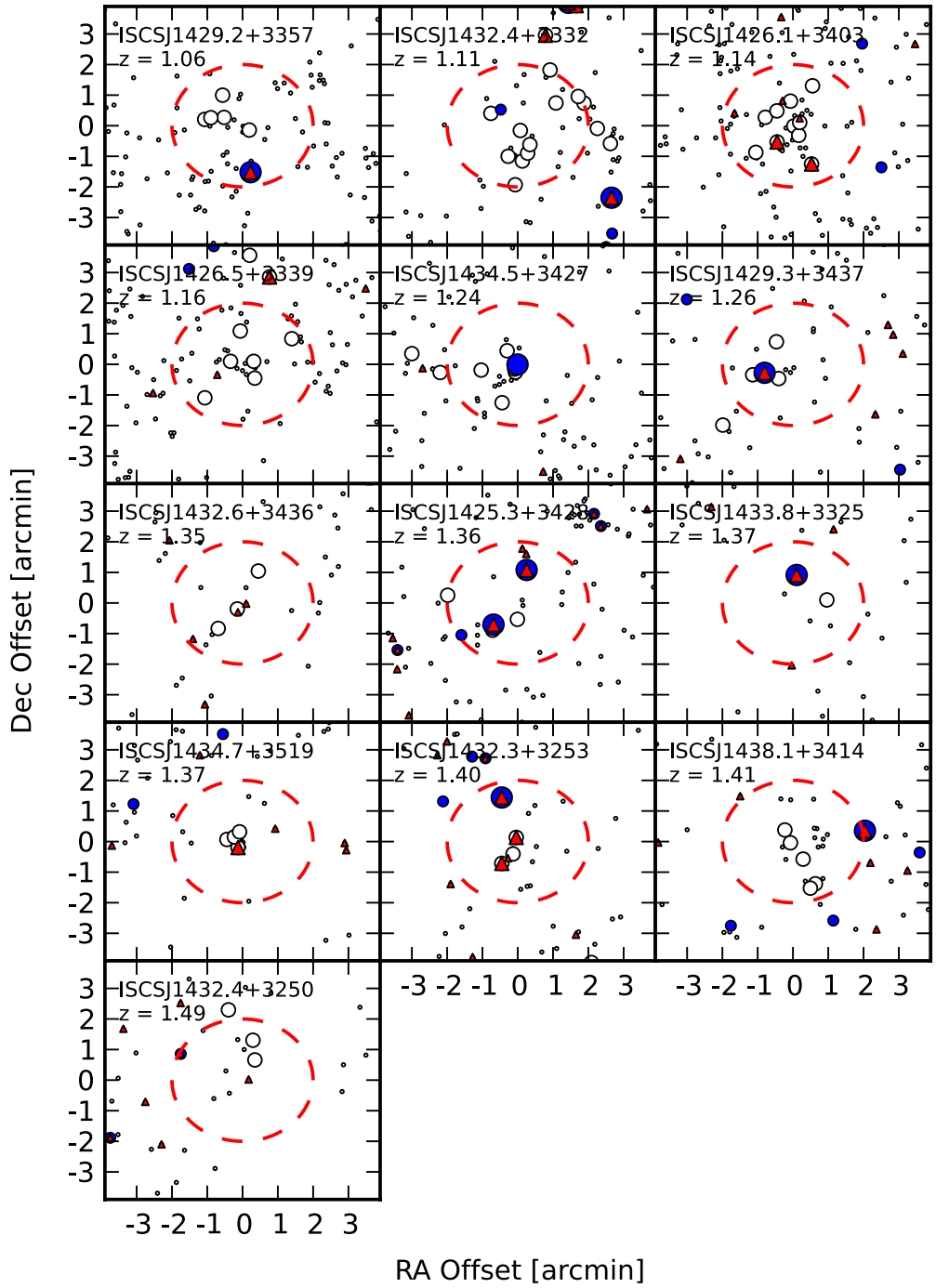

Figure 3. Positions of all cluster galaxies out to a projected distance of 2′ ($\sim r_{200}$, dashed circle) and field galaxies consistent with the cluster redshift within an 8′ × 8′ box centered on the cluster. Only galaxies with photometric uncertainties less than 0.3 mag in the *I* and 3.6 μm bands are shown. Symbols are as in Figures 1 and 2. (A color version of this figure is available in the online journal.)

to all AGNs above a fixed luminosity threshold, but are instead calculated from all AGNs above our detection threshold in galaxies more luminous than $M^*_{3.6} + 1$. An alternative way to express this is to note that the cluster galaxies, cluster galaxies with X-ray coverage, X-ray AGNs, and MIR AGNs correspond to similar overdensities of $(\Sigma - \langle\Sigma\rangle)/\langle\Sigma\rangle = 1.02, 0.87, 0.82,$ and 1.25, respectively. We discuss the significance of the similar cluster and field AGN fractions in Section 6.

There are three biases that influence our estimates. First, the cluster sample has been identified via spectroscopic redshifts, or photometric redshifts if no spectroscopic data are available, while the field sample has almost exclusively been identified via photometric redshifts. As a result of the spectroscopic observations, the surface density of foreground and background contamination within the clusters is lower than it is outside of them. We have compared the number of cluster members within 2′ based on photometric redshifts alone to the number when spectroscopic data are included and find the change is ∼10%, that is we may have slightly underestimated the total number of cluster galaxies that form the denominator of the cluster AGN fraction (this will not affect the relative AGN fraction in the field and clusters). The second bias is that two MIR AGNs were

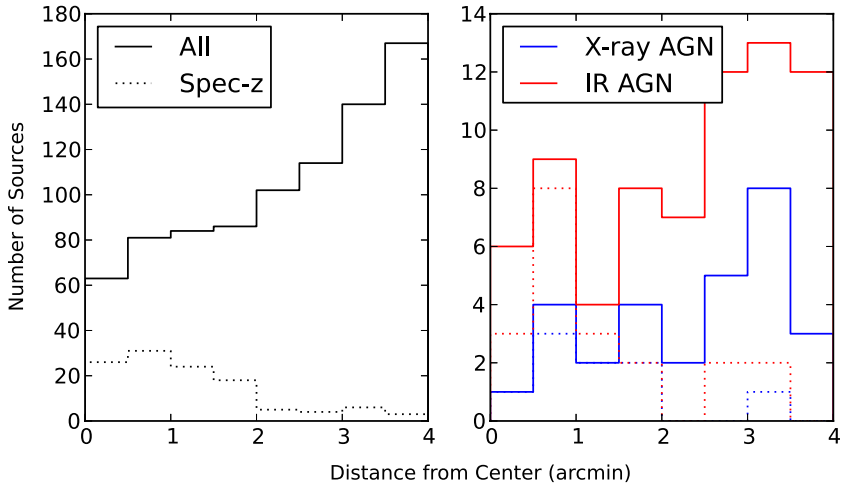

Figure 4. Stacked histograms of the galaxies shown in Figure 3 as a function of clustercentric distance out to 4′. Left: stack of all galaxies with photometric or spectroscopic redshifts (solid line) and only spectroscopic redshifts (dotted line) consistent with cluster membership as a function of projected clustercentric distance. Right: same as the left panel but for the X-ray AGNs (blue lines) and MIR AGNs (red lines) as a function of projected clustercentric distance.

(A color version of this figure is available in the online journal.)

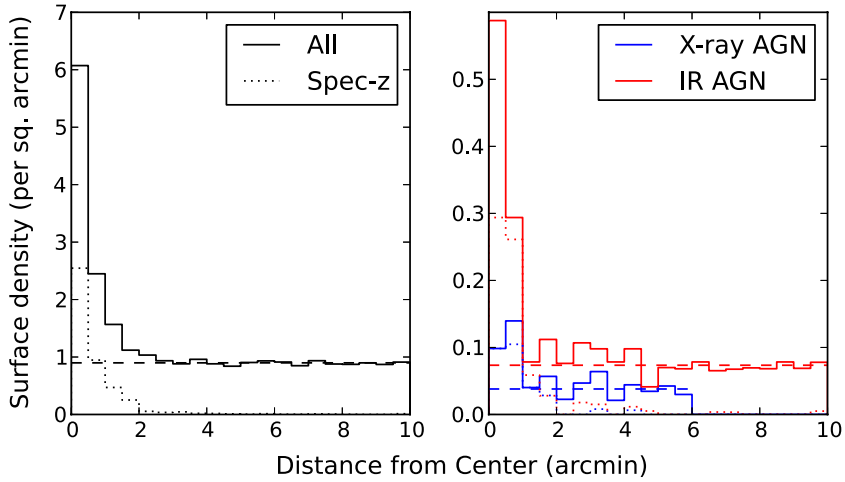

Figure 5. Same as Figure 4, except out to 10′ from the cluster centers and normalized by the area of each annulus to show the density of sources per square arcminute. The dashed, horizontal lines correspond to the median field surface densities calculated from 2′ to 10′ (for all galaxies and IR AGNs), or from 2′ to 6′ (for X-ray AGNs) from the cluster center.

(A color version of this figure is available in the online journal.)

selected as targets for spectroscopy (see Section 3.2) and both are also X-ray AGNs. These constitute only 2 out of 11 X-ray AGNs and 2 out of 27 MIR AGNs, so this selection has a minor impact on the relative cluster and field AGN fractions. This bias does not impact the numerator of the AGN fractions that are derived from spectroscopic redshifts alone. The third bias is that our field region only extends to a projected separation of $3r_{200}$ (X-ray AGNs) to $5r_{200}$ (IR AGNs). The region out to $5r_{200}$ is sometimes referred to as the "infall region" as galaxies at these distances may have been "pre-processed" by membership in an infalling group or have even already passed through the cluster (Diaferio et al. 2001; Patel et al. 2009; Balogh et al. 2009; Bahe et al. 2013) and thus may not be representative of the true field population. We expect that most of the field sample is representative of the true field because the photometric redshifts will include many true foreground and background galaxies in the field sample; nevertheless, our field estimate may be somewhat biased by the infall population.

5. EVOLUTION OF THE AGN FRACTION IN CLUSTERS OF GALAXIES

Of the 11 X-ray AGNs in these clusters, 8 have spectroscopic redshifts that confirm their cluster membership. All of these X-ray AGNs have rest-frame, hard X-ray luminosities greater than $L_{X,H} \geqslant 10^{43}$ erg s^{-1} and four (all with spectroscopic redshifts) have $L_{X,H} \geqslant 10^{44}$ erg s^{-1}. Our X-ray data are sufficiently sensitive that we should have detected all AGNs with $L_{X,H} \geqslant 10^{44}$ erg s^{-1} at the redshifts of these clusters, with the possible exception of AGNs in the chip gaps of the ACIS camera. We have examined exposure maps of these fields and conclude that chip gaps affect at most 5 of the 350 galaxies that are within the area of these clusters and have photometric or spectroscopic redshifts consistent with cluster membership. Therefore a negligible fraction of X-ray AGNs are missed in the chip gaps. In Section 4, we estimated that there are a total of 136 cluster members in galaxies more luminous than $M^*_{3.6} + 1$ with

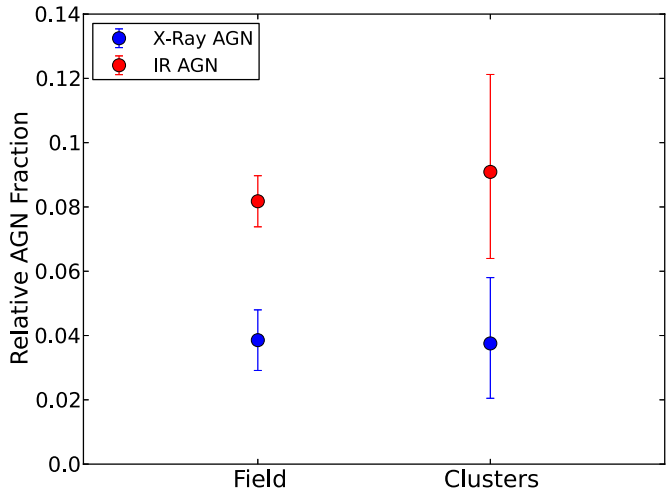

Figure 6. Relative fraction of X-ray AGNs (blue) and MIR AGNs (red) in the field and cluster samples. The error bars correspond to the 90% confidence limits calculated from the relative Poisson uncertainty in the number of AGNs in each subsample. The field sample is comprised of AGNs located 2′–10′ (IR AGNs) and 2′–6′ (X-ray AGNs) from each cluster that have been selected in an otherwise identical manner to the cluster sample.

(A color version of this figure is available in the online journal.)

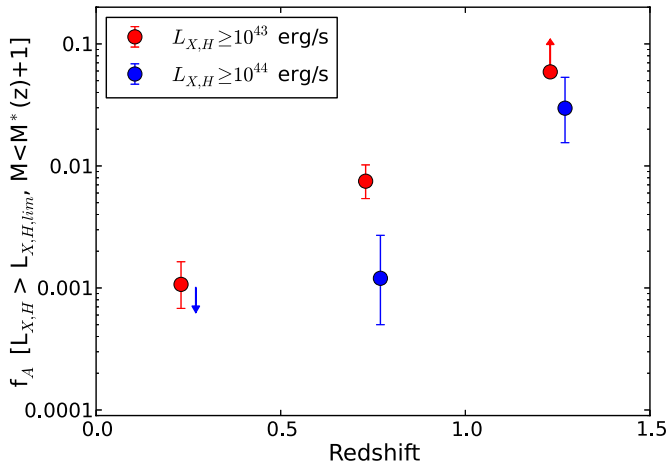

Figure 7. Evolution of the X-ray AGN fraction in clusters from $z = 0$ to $z = 1.5$ for hard X-ray luminosity thresholds of $L_{X,H} \geqslant 10^{43}$ erg s^{-1} (red) and $L_{X,H} \geqslant 10^{44}$ erg s^{-1} (blue). The error bars correspond to 1σ Gaussian errors and the upper limit at $z \sim 0.25$ corresponds to a 3σ upper limit. The lower limit at $z \sim 1.25$ is due to incompleteness.

(A color version of this figure is available in the online journal.)

complete X-ray coverage (after we correct for foreground and background contamination). We therefore estimate that the AGN fraction is $f_A(L_{X,H} \geqslant 10^{44}) = 0.030^{+0.024}_{-0.014}$. The uncertainties are Poisson errors that correspond to 1σ Gaussian confidence intervals (Gehrels 1986).

We are only sensitive to sources as dim as $L_{X,H} \sim 10^{43}$ erg s^{-1} in a small minority of the clusters. As the luminosity function of cluster AGNs is not well known at these luminosities, and variations in the SEDs and intrinsic absorption are similarly not well known, we do not attempt to model and correct these data to estimate the total number of X-ray AGNs with $L_{X,H} \geqslant 10^{43}$. Instead we use our data to establish a lower limit on the cluster AGN fraction for sources with $L_{X,H} \geqslant 10^{43}$ erg s^{-1}. There are 8 spectroscopically confirmed AGNs in this category (and 11 total), for a lower limit of $f_A(L_{X,H} \geqslant 10^{43}) > 0.059^{+0.029}_{-0.021}(0.082^{+0.032}_{-0.024})$. The AGN fractions based on the spectroscopically confirmed AGNs are shown in Figure 7 near $z = 1.26$, the median redshift of the cluster sample (although offset slightly in redshift for clarity).

Both of these measurements imply that luminous X-ray AGNs are more common in clusters at $z > 1$ compared to lower redshifts, as had been indicated by previous work at $z < 1$ (Eastman et al. 2007; Galametz et al. 2009; Martini et al. 2009). Martini et al. (2009) calculated the AGN fraction and evolution in a similar manner to this study for 32 clusters at $0.05 < z < 1.27$ (only three at $z > 1$) and $L_{X,H} \geqslant 10^{43}$ erg s^{-1}. They found that the AGN fraction was $f_A(L_{X,H} \geqslant 10^{43}) = 0.00134$ for $0.05 < z < 0.4$ and 0.0100 for $0.4 < z < 1.27$, where the uncertainty in the measurement at $z < 0.4$ is dominated by the presence of only 2 AGNs in the 17 clusters in this redshift range. We have combined the 19 clusters at $z < 0.5$ presented in Martini et al. (2009) with the more recent study by Haines et al. (2012) of AGNs in clusters at $0.16 < z < 0.29$ to construct a combined sample of 44 clusters and $3869 + 2702 = 6571$ cluster galaxies at $z < 0.5$.[15] Martini et al. (2009) found 4 AGNs (2 with $0.4 < z < 0.5$) with $L_{X,H} \geqslant 10^{43}$ erg s^{-1} (and none with $L_{X,H} \geqslant 10^{44}$ erg s^{-1}). Haines et al. (2012) quote X-ray luminosities in the 0.3–7 keV band, rather than 2–10 keV. We used the ratio of the 0.3–7 keV band to the 2–10 keV band for a $\Gamma = 1.7$ power law to scale their results to 2–10 keV. This yields three AGNs in their sample with $L_{X,H} \geqslant 10^{43}$ erg s^{-1} and none above 10^{44} erg s^{-1}. The combined sample has AGN fractions of $f_A(L_{X,H} \geqslant 10^{43}) = 0.00107^{+0.00057}_{-0.00039}$ and $f_A(L_{X,H} \geqslant 10^{44}) < 0.00101$ (a 3σ upper limit). This point and upper limit are shown in Figure 7 near $z = 0.25$. At intermediate redshifts of $0.5 < z < 1$, Martini et al. (2009) found 13 AGNs with $L_{X,H} \geqslant 10^{43}$ erg s^{-1}, including 2 with $L_{X,H} \geqslant 10^{44}$ erg s^{-1}, in 10 clusters and an estimated population of 1734 galaxies. The AGN fractions are $f_A(L_{X,H} \geqslant 10^{43}) = 0.0075^{+0.0027}_{-0.0021}$ and $f_A(L_{X,H} \geqslant 10^{44}) = 0.0012^{+0.0015}_{-0.0007}$. These points are shown in Figure 7 near $z = 0.75$. Note the luminosity thresholds employed to define the galaxy samples in these studies are similar to ours: Martini et al. (2009) adopted a threshold of $M^*_R(z)+1$ and Haines et al. (2012) adopted $M^*_K+1.5$.

The evolution in the AGN fraction corresponds to a factor of at least 45 for $L_{X,H} \geqslant 10^{43}$ erg s^{-1} AGNs from $z \sim 0.25$ to $z \sim 1.25$ and a factor of at least 30 for $L_{X,H} \geqslant 10^{44}$ erg s^{-1} AGNs. In the former case, the increase is a lower limit due to incompleteness at $z > 1$. In the latter case the increase is a lower limit due to the absence of any AGN in this luminosity range in the 44 clusters that comprise the low-redshift sample. For the two luminosity and redshift ranges without limits on the fractions, the evolution in the AGN fraction is also pronounced. For $L_{X,H} \geqslant 10^{43}$ erg s^{-1} AGNs, the fraction increases by a factor of seven over the range $0.25 < z < 0.75$. For $L_{X,H} \geqslant 10^{44}$ erg s^{-1} AGNs, the fraction increases by a factor of 25 over the range $0.75 < z < 1.25$. This substantial increase is in good agreement with the increase over this same redshift range found by Galametz et al. (2009) and Hart et al. (2011), although for a somewhat different range in luminosities.

Two complications in the interpretation of the evolution of the AGN fraction are the extent to which the high-redshift clusters are equivalent to the progenitors of the low-redshift clusters and the incompleteness and evolution of the cluster galaxies. If the AGN fraction is a strong function of cluster mass, in addition

[15] Many of the clusters at $0.2 < z < 0.4$ studied by Hart et al. (2009) overlap with either the Martini et al. (2009) or Haines et al. (2012) sample. Only one cluster (A1689) overlaps between Martini et al. (2009) and Haines et al. (2012).

to redshift, then mass dependence could manifest as redshift dependence. Based on previous analysis of the $1 < z < 1.5$ sample (Brodwin et al. 2007, 2011; Jee et al. 2011), these clusters are expected to be the high-redshift progenitors of present-day $10^{15}\ M_{\odot}$ clusters such as Coma. The cluster samples in the range $0 < z < 1$ studied by Martini et al. (2009) are similarly massive and consistent with the same population of clusters in the local universe. Similarity to Coma was explicitly used by Hart et al. (2009) to select their sample, which overlaps with the other low-redshift cluster samples. To the extent that there is a bias in these data, the higher-redshift clusters tend to be slightly more massive. As there is an anticorrelation between luminous AGNs and environment in the local universe (Kauffmann et al. 2004), this anticorrelation would produce an underestimate of the true rate of evolution.

The other complication originates in the comparison of the cluster galaxy populations across different surveys and from the local universe to $z = 1.5$. In this study we have focused on the AGN fraction for cluster galaxies more luminous than 1 mag below the knee of the luminosity function at the cluster redshift. This choice was motivated by the previous study by Martini et al. (2009) who adopted the assumption that $M_R^*(z) = M_R^*(0) - z$. Haines et al. (2012) adopted a similar threshold for the galaxy population, although their galaxy luminosity threshold was 1.5 mag below the knee of the luminosity function (defined in the K band: $M_K^* + 1.5$). We estimate that the half magnitude difference for the galaxy population is a minor effect compared to the Poisson uncertainties, as the $z < 0.5$ AGN fractions measured by these two studies are consistent. At intermediate redshifts $0.5 < z < 1$ the cluster spectroscopic data are incomplete for galaxies (although not for the much smaller number of X-ray sources), and there is thus a substantial correction to estimate the total galaxy population of some clusters. Martini et al. (2009) investigated this effect and estimated that it introduced on order a factor of two uncertainty into the AGN fraction estimate at $z > 0.5$, which is much smaller than the observed evolution. While the present sample at $1 < z < 1.5$ similarly suffers from spectroscopic incompleteness, the high-quality photometric redshifts, substantial sample of field galaxies, and availability of some spectroscopic follow-up substantially mitigate this uncertainty such that the cluster galaxy population is probably more reliably known for the present sample than for the sample at $0.5 < z < 1$.

6. DISCUSSION

The field X-ray AGN fraction also increases over the same redshift range of $0 < z < 1.5$ where the cluster AGN fraction has increased by factors of at least 30–45 (e.g., Ueda et al. 2003). At $z \sim 1.25$, we showed in Section 4 and Figure 6 that the cluster and field AGN fractions were comparable and both $\sim$3%–4% for AGNs with hard X-ray luminosities greater than a few times 10^{43} erg s^{-1}. Because our field measurement is from the immediate vicinity of massive clusters, some of the field galaxies may have already been processed through the cluster (e.g., Diaferio et al. 2001; Patel et al. 2009; Balogh et al. 2009; Bahe et al. 2013) and the field sample may not be representative of the true field population. Another estimate of the field AGN fraction at these redshifts was presented by Bundy et al. (2008) from an analysis of galaxies and AGNs in the DEEP2 survey. They found that the AGN fraction is $\sim$1%–3% for AGNs with $L_{X,H} > 10^{43}$ erg s^{-1} in host galaxies with stellar masses of $M_* \sim 10^{11.5}$ at $1 < z < 1.4$. This fraction appears consistent with our measurement for the field fraction around the clusters, although our data do not extend to $L_{X,H} = 10^{43}$ erg s^{-1} for most clusters and the stellar mass range quoted by Bundy et al. (2008) is not an exact match to our luminosity threshold at 3.6 μm.

In the local universe, very luminous AGNs are rarely found in the field and very rarely found in clusters. A Sloan Digital Sky Survey (SDSS) study by Kauffmann et al. (2004) found that AGNs with $L[\mathrm{O\ III}] > 10^7\ L_{\odot}$ were approximately three times rarer in dense environments relative to less dense environments, where this luminosity threshold is approximately comparable to an AGN with $L_{X,H} = 10^{43}$ erg s^{-1}. A factor of three to four decrease in the AGN fraction with the same luminosity threshold was also found by Best et al. (2005b) over an order of magnitude change in local density with data from SDSS. However, both studies also find little environmental dependence in the AGN fraction when only lower-luminosity AGNs were examined. Note that for both of these studies, the high-density regions are still not as dense as the centers of rich clusters of galaxies, which are embedded in very rare and very massive dark matter halos (on order $10^{15}\ M_{\odot}$) in the local universe.

The local field X-ray AGN fraction was measured by Haggard et al. (2010) based on data from the *Chandra* Multiwavelength Project (ChaMP; Green et al. 2004) and SDSS, although they do not use hard X-ray luminosities and probe a somewhat different range in galaxy luminosity and redshift. Haggard et al. (2010) compared their results to previous cluster studies (Martini et al. 2006, 2007) and found the field and cluster AGN fractions are the same for low-luminosity AGNs ($L_X > 10^{41-42}$ erg s^{-1}). Other studies have reached similar conclusions, namely, the fraction of low-luminosity AGNs is comparable in clusters, groups, and the field in the local universe (Sivakoff et al. 2008; Arnold et al. 2009; Miller et al. 2012). The sample studied by Haggard et al. (2010) also includes some higher-luminosity AGNs that are more directly comparable to the AGN considered here. D. Haggard (2012, private communication) has computed the field AGN fraction for similar X-ray and galaxy luminosity limits for $0 < z < 0.6$ and found $f_A(L_{X,H} > 10^{43}) = 0.0064^{+0.0004}_{-0.0005}$ and $f_A(L_{X,H} > 10^{44}) = 0.0011^{+0.0002}_{-0.0002}$. These points are shown in Figure 8 (note the formal uncertainties are smaller than the points) and demonstrate that the $L_{X,H} > 10^{43}$ erg s^{-1} field AGN fraction is six times higher than the cluster value and the $L_{X,H} > 10^{44}$ erg s^{-1} field AGN fraction is consistent with the 3σ upper limit for the cluster AGN fraction. While the two field fractions at $z \sim 0.3$ are calculated with the ChaMP survey's definition of the hard band of 2–8 keV, rather than the 2–10 keV band adopted in this paper, this is a very minor difference. The relative field and cluster AGN fractions in the local universe at $z \sim 1.25$ show that while luminous AGNs are anticorrelated with local density in the local universe, this is no longer the case at $z \sim 1.25$. The masses of these high-redshift clusters are also in the range expected for the progenitors of the local clusters.

Studies at even higher redshift support this trend and suggest that the present-day anticorrelation has reversed by $z > 2$. *Chandra* observations of three protoclusters at $z > 2$ have revealed luminous AGNs associated with PKS 1138−262 at $z = 2.16$ (Pentericci et al. 2002; Croft et al. 2005), the $z = 2.3$ protocluster in the field of QSO HS 1700+643 (Digby-North et al. 2010), and the $z = 3.09$ SSA22 protocluster (Lehmer et al. 2009). Pentericci et al. (2002) compared the number of sources toward PKS 1138−262 and found an excess of $\sim$50% compared to expectations from the AGN space density at this redshift. Lehmer et al. (2009) and Digby-North et al. (2010) both measure the AGN fractions of the protoclusters and in field samples at the same redshift. Lehmer et al. (2009) detected X-ray

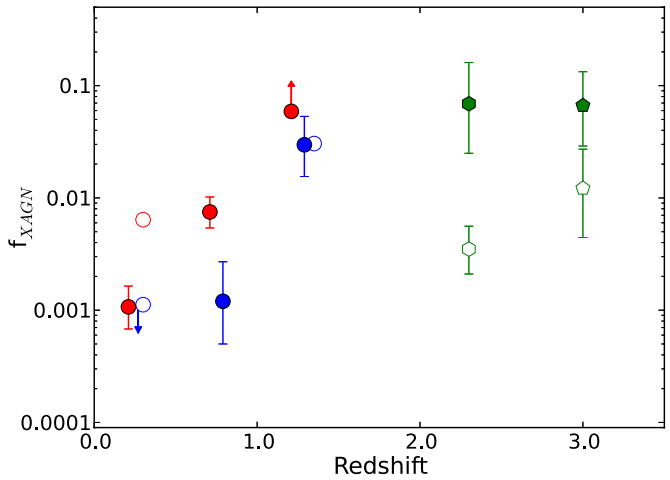

Figure 8. Evolution of the X-ray AGN fraction in clusters (solid symbols) and the field (open symbols) from $z = 0$ to $z \sim 3$. All of the cluster measurements have been reproduced from Figure 7. The field AGN fractions at $z \sim 0.3$ for $L_{X,H} \geqslant 10^{43}$ erg s^{-1} (open, red circles) and $L_{X,H} \geqslant 10^{44}$ erg s^{-1} (open, blue circles) are from D. Haggard (2012, private communication; see also Haggard et al. 2010). The formal uncertainties on these two field fractions are smaller than the size of the circles. The field AGN point at $z \sim 1.25$ (open blue circle) is scaled from the cluster point by the ratio of the field and cluster fractions shown in Figure 6. The $z = 2.3$ protocluster and neighboring field fractions from Digby-North et al. (2010; filled and open green hexagons, respectively) and the $z = 3.09$ protocluster and neighboring field fractions from Lehmer et al. (2009; filled and open green pentagons, respectively) are also shown. These points are described further in Section 6.

(A color version of this figure is available in the online journal.)

emission from 6 Lyman-break galaxy (LBGs) and 5 Lyman α-emitter (LAEs) (10 unique sources) toward the SSA22 protocluster at $z = 3.09$ with a 400 ks *Chandra* observation. These sources have X-ray luminosities of 3–50 $\times$ 10^{43} erg s^{-1} in the rest-frame 8–32 keV band. They measure AGN fractions of $9.5^{+12.7}_{-6.1}$% and $5.1^{+6.8}_{-3.3}$% in LBGs and LAEs, respectively. These AGN fractions are larger by a factor of $6.1^{+10.3}_{-3.6}$ compared to the lower-density field at the same redshift. Digby-North et al. (2010) studied the $z = 2.30$ protocluster in the field of QSO HS 1700+643 and found five protocluster AGNs in their ~200 ks *Chandra* observation. They identified AGNs with $L_{X,H} \geqslant 4.6 \times 10^{43}$ erg s^{-1} in a sample of members selected via the BX/MD method and as LAEs. The X-ray AGN fractions in the BX/MD and LAE samples are $6.9^{+9.2}_{-4.4}$ and $2.9^{+2.9}_{-1.6}$%, respectively, which are greater than the field fractions in similar galaxies at this redshift, particularly for the BX/MD sample. The protocluster and field fractions measured by Lehmer et al. (2009) and Digby-North et al. (2010, for BX/MD galaxies) are shown on Figure 8. While the field fractions for these high-redshift fields are measured in their immediate vicinity, this should be less important than for our sample because both less time has elapsed for environmental pre-processing and the environments are not as evolved.

These data on the evolution of the AGN fraction in the field, clusters, and protoclusters, while heterogeneous with respect to X-ray sensitivity thresholds, cluster selection, and host galaxy properties, broadly indicate that luminous AGNs are anticorrelated with density in the local universe, found in cluster and field galaxies with approximately equal frequency at $1 < z < 1.5$, and are correlated with local density by $z > 2$. This relative evolution of the fraction of luminous AGNs in field and cluster galaxies is consistent with the now-conventional picture that the most luminous AGNs are fueled by gas-rich galaxy mergers (Sanders et al. 1988) and the steady decline in the cold gas content of galaxies from high redshift to the present day. At the highest redshifts discussed here, which correspond to the redshifts of the protoclusters at $2 < z < 3.1$, a larger fraction of the baryonic mass fraction of massive galaxies is in molecular gas compared to their local analogs (Tacconi et al. 2010). The overdense protocluster environment leads to greater likelihood of interactions and mergers of these gas-rich galaxies and thus the fueling of luminous AGNs. By $1 < z < 1.5$, the most overdense cluster environments have grown substantially and are large enough to have substantial hot gas reservoirs, as illustrated by the detection of extended X-ray emission from some clusters at $z > 1$ (Gobat et al. 2011; Brodwin et al. 2011; Stanford et al. 2012). While there is still substantial star formation in many cluster members, including clusters in the present sample (M. Brodwin et al. 2013, in preparation), many other cluster galaxies have stopped substantial star formation, as indicated by the presence of a color–magnitude relation (Mei et al. 2009). This transition is likely because they have largely exhausted their cold gas supply. The increase in the cross section for galaxy interactions and mergers in the cluster environment is consequently counterbalanced by the smaller fraction of gas-rich galaxies, except perhaps on the outskirts of clusters (Wagg et al. 2012). Even at redshift $0.9 < z < 1.6$ there is some evidence for an enhancement of AGNs in the infall region (Fassbender et al. 2012). By the present day, cluster galaxies have much less cold gas compared to field galaxies (Giovanardi et al. 1983; Oosterloo et al. 2010) and the relative velocities of their member galaxies are too great to produce bound pairs that eventually merge. Aside from the central cluster galaxy, which is likely fueled by gas cooling from the intracluster medium, luminous AGNs may only be found in present-day clusters due to the infall of gas-rich field galaxies (Haines et al. 2012). This result is similar to the properties of star-forming galaxies in clusters (Dressler et al. 1999).

7. SUMMARY

We have investigated the X-ray and MIR-selected AGN population in a sample of 13 clusters at $1 < z < 1.5$ identified by the *Spitzer*/ISCS of Eisenhardt et al. (2008). We find a total of 11 X-ray counterparts to cluster members, 8 of which have spectroscopic redshifts. There are also 27 MIR AGNs associated with cluster members, 12 of which have spectroscopic redshifts. All but three of the X-ray AGNs are also MIR AGNs.

The X-ray AGNs are quite luminous. All of the X-ray AGNs have rest-frame, hard X-ray luminosities of $L_{X,H} > 10^{43}$ erg s^{-1} and four have $L_{X,H} > 10^{44}$ erg s^{-1}. AGNs at these luminosities are extremely rare in low-redshift clusters, and in fact none have been found above $L_{X,H} > 10^{44}$ erg s^{-1} in a combined sample of 44 clusters at $z < 0.5$ that we constructed from studies by Martini et al. (2009) and Haines et al. (2012). These new observations demonstrate that the order of magnitude increase in the cluster AGN fraction from the present to $z \sim 1$ continues to $z \sim 1.5$.

We have used photometric redshift estimates for galaxies out to five times the expected r_{200} radius of the clusters, or $R = 2'$–$10'$ from the cluster centers, to characterize the field population and likely field contamination due to the use of photometric redshifts to estimate cluster membership. These observations clearly indicate a substantial excess of galaxies, X-ray AGNs, and MIR AGNs associated with the clusters. We calculate the X-ray and MIR AGN fractions of all galaxies brighter than $M^*_{3.6} + 1$, where $M^*_{3.6}$ corresponds to the knee

of the luminosity function at the cluster redshift. We find that the field AGN fractions, defined from the sample of galaxies at the cluster redshift, but from $R = 2'$–$6'$ (X-ray AGNs) or $R = 2'$–$10'$ (IR AGNs) from the cluster center, are consistent with the cluster AGN fractions within $R \leqslant 2'$. This stands in sharp contrast to estimates at low redshift, where the luminous X-ray AGN fraction is substantially lower in clusters relative to the field (e.g., Martini et al. 2009; Haggard et al. 2010).

The order of magnitude evolution of the cluster AGN fraction from $z = 0$ to $z \sim 1.25$ is greater than the rate of evolution of the field AGN fraction. While the luminous AGN fraction is approximately six times higher in the field than in clusters in the local universe, we find comparable fractions in the field and clusters at $z \sim 1.25$. Studies of two protoclusters and samples of field galaxies at even higher redshifts indicate that the luminous AGN fraction is higher in protoclusters than the field at $z > 2$ (Lehmer et al. 2009; Digby-North et al. 2010). Taken together, these studies and our own demonstrate that there is a reversal of the local anticorrelation between luminous AGNs and local density at high redshift. The relative evolution of the AGN fraction in the field and clusters is strong evidence of environment-dependent AGN evolution.

We thank Daryl Haggard for calculating the field AGN fraction based on our AGN and galaxy luminosity thresholds. We also appreciate a thoughtful and helpful review from the referee. P.M. appreciates support from the sabbatical visitor program at the North American ALMA Science Center (NAASC) at NRAO and the hospitality of both the NAASC and the University of Virginia while this work was completed. The work of P.R.M.E. and D.S. was carried out at the Jet Propulsion Laboratory, California Institute of Technology, under a contract with NASA. Part of this work was performed under the auspices of the U.S. Department of Energy by Lawrence Livermore National Laboratory under Contract DE-AC52-07NA27344. Support for this work was provided by the National Aeronautics and Space Administration through Chandra Award Number GO9-0150A issued by the Chandra X-Ray Observatory Center, which is operated by the Smithsonian Astrophysical Observatory for and on behalf of the National Aeronautics Space Administration under contract NAS8-03060.

Facilities: Spitzer, *CXO*

REFERENCES

Aird, J., Coil, A. L., Moustakas, J., et al. 2012, ApJ, 746, 90
Alonso-Herrero, A., Pérez-González, P. G., Rieke, G. H., et al. 2008, ApJ, 677, 127
Arnold, T. J., Martini, P., Mulchaey, J. S., Berti, A., & Jeltema, T. E. 2009, ApJ, 707, 1691
Ashby, M. L. N., Stern, D., Brodwin, M., et al. 2009, ApJ, 701, 428
Assef, R. J., Kochanek, C. S., Brodwin, M., et al. 2010, ApJ, 713, 970
Atlee, D. W., & Martini, P. 2012, ApJ, 761, 114
Atlee, D. W., Martini, P., Assef, R. J., Kelson, D. D., & Mulchaey, J. S. 2011, ApJ, 729, 22
Bahe, Y. M., McCarthy, I. G., Balogh, M. L., & Font, A. S. 2013, MNRAS
Balogh, M. L., McGee, S. L., Wilman, D., et al. 2009, MNRAS, 398, 754
Barger, A. J., Cowie, L. L., Mushotzky, R. F., et al. 2005, AJ, 129, 578
Barnes, J. E., & Hernquist, L. E. 1991, ApJL, 370, L65
Best, P. N., Kauffmann, G., Heckman, T. M., et al. 2005a, MNRAS, 362, 25
Best, P. N., Kauffmann, G., Heckman, T. M., & Ivezić, Ž. 2005b, MNRAS, 362, 9
Boyle, B. J., Georgantopoulos, I., Blair, A. J., et al. 1998, MNRAS, 296, 1
Brodwin, M., Brown, M. J. I., Ashby, M. L. N., et al. 2006, ApJ, 651, 791
Brodwin, M., Gonzalez, A. H., Moustakas, L. A., et al. 2007, ApJL, 671, L93
Brodwin, M., Stern, D., Vikhlinin, A., et al. 2011, ApJ, 732, 33
Broos, P. S., Townsley, L. K., Feigelson, E. D., et al. 2010, ApJ, 714, 1582
Bundy, K., Georgakakis, A., Nandra, K., et al. 2008, ApJ, 681, 931
Butcher, H., & Oemler, A. 1978, ApJ, 219, 18
Cappelluti, N., Cappi, M., Dadina, M., et al. 2005, A&A, 430, 39
Carlberg, R. G., Yee, H. K. C., & Ellingson, E. 1997, ApJ, 478, 462
Cowie, L. L., & Songaila, A. 1977, Natur, 266, 501
Croft, S., Kurk, J., van Breugel, W., et al. 2005, AJ, 130, 867
Demarco, R., Rosati, P., Lidman, C., et al. 2005, A&A, 432, 381
Diaferio, A., Kauffmann, G., Balogh, M. L., et al. 2001, MNRAS, 323, 999
Digby-North, J. A., Nandra, K., Laird, E. S., et al. 2010, MNRAS, 407, 846
Donley, J. L., Koekemoer, A. M., Brusa, M., et al. 2012, ApJ, 748, 142
Dressler, A. 1980, ApJ, 236, 351
Dressler, A., & Gunn, J. E. 1983, ApJ, 270, 7
Dressler, A., Smail, I., Poggianti, B. M., et al. 1999, ApJS, 122, 51
Dressler, A., Thompson, I. B., & Shectman, S. A. 1985, ApJ, 288, 481
Eastman, J., Martini, P., Sivakoff, G., et al. 2007, ApJL, 664, L9
Eckart, M. E., Stern, D., Helfand, D. J., et al. 2006, ApJS, 165, 19
Eisenhardt, P. R., Stern, D., Brodwin, M., et al. 2004, ApJS, 154, 48
Eisenhardt, P. R. M., Brodwin, M., Gonzalez, A. H., et al. 2008, ApJ, 684, 905
Elbaz, D., Daddi, E., Le Borgne, D., et al. 2007, A&A, 468, 33
Elmegreen, B. G., Elmegreen, D. M., Brinks, E., et al. 1998, ApJL, 503, L119
Elston, R. J., Gonzalez, A. H., McKenzie, E., et al. 2006, ApJ, 639, 816
Farouki, R., & Shapiro, S. L. 1981, ApJ, 243, 32
Fassbender, R., Šuhada, R., & Nastasi, A. 2012, AdAst, 2012, 32
Ferrarese, L., & Merritt, D. 2000, ApJL, 539, L9
Franceschini, A., Hasinger, G., Miyaji, T., & Malquori, D. 1999, MNRAS, 310, L5
Fuentes-Williams, T., & Stocke, J. T. 1988, AJ, 96, 1235
Galametz, A., Stern, D., Eisenhardt, P. R. M., et al. 2009, ApJ, 694, 1309
Gebhardt, K., Bender, R., Bower, G., et al. 2000, ApJL, 539, L13
Gehrels, N. 1986, ApJ, 303, 336
Genzel, R., Burkert, A., Bouché, N., et al. 2008, ApJ, 687, 59
Gilmour, R., Best, P., & Almaini, O. 2009, MNRAS, 329, 1509
Giovanardi, C., Krumm, N., & Salpeter, E. E. 1983, AJ, 88, 1719
Giovanelli, R., & Haynes, M. P. 1985, ApJ, 292, 404
Gisler, G. R. 1978, MNRAS, 183, 633
Gobat, R., Daddi, E., Onodera, M., et al. 2011, A&A, 526, A133
Gralla, M. B., Gladders, M. D., Yee, H. K. C., & Barrientos, L. F. 2011, ApJ, 734, 103
Green, P. J., Silverman, J. D., Cameron, R. A., et al. 2004, ApJS, 150, 43
Gunn, J. E., & Gott, J. R. I. 1972, ApJ, 176, 1
Haggard, D., Green, P. J., Anderson, S. F., et al. 2010, ApJ, 723, 1447
Haines, C. P., Pereira, M. J., Sanderson, A. J. R., et al. 2012, ApJ, 754, 97
Haines, C. P., Smith, G. P., Egami, E., et al. 2009, ApJ, 704, 126
Hart, Q. N., Stocke, J. T., Evrard, A. E., Ellingson, E. E., & Barkhouse, W. A. 2011, ApJ, 740, 59
Hart, Q. N., Stocke, J. T., & Hallman, E. J. 2009, ApJ, 705, 854
Hasinger, G., Miyaji, T., & Schmidt, M. 2005, A&A, 441, 417
Heckman, T. M., Kauffmann, G., Brinchmann, J., et al. 2004, ApJ, 613, 109
Hickox, R. C., Jones, C., Forman, W. R., et al. 2009, ApJ, 696, 891
Hilton, M., Lloyd-Davies, E., Stanford, S. A., et al. 2010, ApJ, 718, 133
Hopkins, P. F., Hernquist, L., Cox, T. J., et al. 2006, ApJS, 163, 1
Hopkins, P. F., & Quataert, E. 2011, MNRAS, 415, 1027
Jannuzi, B. T., & Dey, A. 1999, in ASP Conf. Ser. 191, Photometric Redshifts and the Detection of High Redshift Galaxies, ed. R. Weymann, L. Storrie-Lombardi, M. Sawicki, & R. Brunner (San Francisco, CA: ASP), 111
Jee, M. J., Dawson, K. S., Hoekstra, H., et al. 2011, ApJ, 737, 59
Johnson, O., Best, P. N., & Almaini, O. 2003, MNRAS, 343, 924
Kauffmann, G., Heckman, T. M., Tremonti, C., et al. 2003, MNRAS, 346, 1055
Kauffmann, G., White, S. D. M., Heckman, T. M., et al. 2004, MNRAS, 353, 713
Kelson, D. D., van Dokkum, P. G., Franx, M., Illingworth, G. D., & Fabricant, D. 1997, ApJL, 478, L13
Kenter, A., Murray, S. S., Forman, W. R., et al. 2005, ApJS, 161, 9
Kochanek, C. S., Eisenstein, D. J., Cool, R. J., et al. 2012, ApJS, 200, 8
Lacy, M., Storrie-Lombardi, L. J., Sajina, A., et al. 2004, ApJS, 154, 166
Larson, R. B., Tinsley, B. M., & Caldwell, C. N. 1980, ApJ, 237, 692
Lehmer, B. D., Alexander, D. M., Geach, J. E., et al. 2009, ApJ, 691, 687
Mancone, C. L., Gonzalez, A. H., Brodwin, M., et al. 2010, ApJ, 720, 284
Martini, P. 2004, in IAU Symp., The Interplay among Black Holes, Stars and ISM in Galactic Nuclei, ed. T. Storchi-Bergmann, L. C. Ho, & H. R. Schmitt (Cambridge: Cambridge Univ. Press), 235
Martini, P., Kelson, D. D., Kim, E., Mulchaey, J. S., & Athey, A. A. 2006, ApJ, 644, 116
Martini, P., Kelson, D. D., Mulchaey, J. S., & Trager, S. C. 2002, ApJL, 576, L109
Martini, P., Mulchaey, J. S., & Kelson, D. D. 2007, ApJ, 664, 761
Martini, P., Regan, M. W., Mulchaey, J. S., & Pogge, R. W. 2003, ApJ, 589, 774

Martini, P., Sivakoff, G. R., & Mulchaey, J. S. 2009, ApJ, 701, 66
Mei, S., Holden, B. P., Blakeslee, J. P., et al. 2009, ApJ, 690, 42
Merloni, A., Rudnick, G., & Di Matteo, T. 2004, MNRAS, 354, L37
Merritt, D. 1983, ApJ, 264, 24
Miller, C. J., Nichol, R. C., Gómez, P. L., Hopkins, A. M., & Bernardi, M. 2003, ApJ, 597, 142
Miller, E. D., Bautz, M., Forman, W., et al. 2012, BAAS, 220, 435.04
Moore, B., Katz, N., Lake, G., Dressler, A., & Oemler, A., Jr. 1996, Natur, 379, 613
Mulchaey, J. S., & Regan, M. W. 1997, ApJL, 482, L135
Murray, S. S., Kenter, A., Forman, W. R., et al. 2005, ApJS, 161, 1
Oosterloo, T., Morganti, R., Crocker, A., et al. 2010, MNRAS, 409, 500
Patel, S. G., Kelson, D. D., Holden, B. P., et al. 2009, ApJ, 694, 1349
Pentericci, L., Kurk, J. D., Carilli, C. L., et al. 2002, A&A, 396, 109
Popesso, P., & Biviano, A. 2006, A&A, 460, L23
Richstone, D. O. 1976, ApJ, 204, 642
Rumbaugh, N., Kocevski, D. D., Gal, R. R., et al. 2012, ApJ, 746, 155
Saintonge, A., Tran, K.-V. H., & Holden, B. P. 2008, ApJL, 685, L113
Sanders, D. B., Soifer, B. T., Elias, J. H., et al. 1988, ApJ, 325, 74
Silverman, J. D., Green, P. J., Barkhouse, W. A., et al. 2008, ApJ, 679, 118
Simkin, S. M., Su, H. J., & Schwarz, M. P. 1980, ApJ, 237, 404
Sivakoff, G. R., Martini, P., Zabludoff, A. I., Kelson, D. D., & Mulchaey, J. S. 2008, ApJ, 682, 803
Stanford, S. A., Brodwin, M., Gonzalez, A. H., et al. 2012, ApJ, 753, 164
Stanford, S. A., Eisenhardt, P. R., Brodwin, M., et al. 2005, ApJL, 634, L129
Stern, D., Eisenhardt, P., Gorjian, V., et al. 2005, ApJ, 631, 163
Tacconi, L. J., Genzel, R., Neri, R., et al. 2010, Natur, 463, 781
Tanaka, M., Finoguenov, A., Mirkazemi, M., et al. 2012, PASJ, in press (arXiv:1210.0302)
Terlevich, E., Diaz, A. I., & Terlevich, R. 1990, MNRAS, 242, 271
Tran, K.-V. H., Papovich, C., Saintonge, A., et al. 2010, ApJL, 719, L126
Tremaine, S., Gebhardt, K., Bender, R., et al. 2002, ApJ, 574, 740
Ueda, Y., Akiyama, M., Ohta, K., & Miyaji, T. 2003, ApJ, 598, 886
van Dokkum, P. G., & Franx, M. 1996, MNRAS, 281, 985
Veilleux, S., Rupke, D. S. N., Kim, D.-C., et al. 2009, ApJS, 182, 628
Wagg, J., Pope, A., Alberts, S., et al. 2012, ApJ, 752, 91
Zeimann, G. R., Stanford, S. A., Brodwin, M., et al. 2012, ApJ, 756, 115